Increasing the Trapping Efficiency of Particles in Microfluidic Planar Platforms by Means of Negative Dielectrophoresis

Fabrice Gielen,[†,‡,§] Andrew J. deMello,[‡] Tony Cass,[†] and Joshua B. Edel*[,†,‡]

Department of Chemistry, Institute of Biomedical Engineering, and Chemical Biology Centre, Imperial College London, South Kensington, London, SW7 2AZ, United Kingdom

Received: October 08, 2008; Revised Manuscript Received: November 12, 2008

We present a novel planar electrode geometry in which particles (typically 10 μm in diameter) are focused near a defined surface before being trapped using negative dielectrophoresis. The focusing element can deflect particles having speeds up to hundreds of micrometers per second. This trapping configuration results in improved trapping yields and a decrease in overall reagent consumption. Particles are trapped dynamically while flowing in a microfluidic channel.

Introduction

The handling of individual particles in a microfluidic environment includes several manipulation techniques including filtering, focusing, trapping, and sorting.[1] Focusing refers to the deviation of particles toward a chosen convergence location. This is the key principle used in flow cytometry but it also finds applications in the separation of dielectric particles.[2,3] Importantly, this focusing step is extremely valuable when working with biological samples having low analyte concentration or when a subsequent detection technique assumes a particle flow over a small detection volume.

Focusing particles in contact or close to a defined surface can find applications in diagnostics (e.g., heterogeneous immunoassays),[4,5] combinatorial chemistry based on particle manipulation,[6,7] or cell biology, especially cellular membrane studies.[8,9] Generally speaking, the motion of particles in contact or in the vicinity of a surface can be used for particle−surface interaction studies. For example, the amount of contact a cellular membrane can have with a defined surface could be controlled and subsequently used to examine change in the local mechanical properties of a lipid bilayer. Furthermore focusing of particles at a single plane level is especially useful when followed by trapping due to planar electrodes rarely reach 100% focusing yields (number of particles actually focused/total number of flowing particles) due to the limited electric field extension away from electrodes.

The particle manipulation techniques aforementioned can be performed using dielectrophoresis (DEP) and integrated on a single laboratory-on-a-chip platform.[1−3,10−12] Dielectrophoresis typically uses nonuniform AC electric fields (10 kHz to 100 MHz) to position particles guided by an electric field gradient.[13] DEP exerts dipolar forces on dielectric particles such as microbeads or cells. If the medium is more polarizable than the particle, the force brings the particle away from high field regions; this is referred to as negative dielectrophoresis (repulsion forces). In the case of nonconductive dielectric particles or cells in physiological high conductivity medium, negative DEP (nDEP) is always obtained. In addition to beads, DEP is extremely well suited for cellular manipulation due to the specific polarization responses to a high frequency electric field.[14−17] Furthermore it has been shown that cells can be cultured even under permanently applied fields.[17]

Focusing near a Surface with DEP. Focusing can be achieved using both positive and negative DEP.[18,19] In many articles utilizing DEP focusing, particles are moved to the geometric center of a microchannel.[1,3,10−12] This is usually achieved using two aligned planar electrodes on both the bottom and ceiling of a fluidic channel. Hydrodynamic focusing has been investigated but cannot easily confine particles down to a surface.[3] Few studies rely on three-dimensional (3D) fabrication techniques to build 3D electrodes[12] as the fabrication of these geometries is difficult due to multilayer alignment and packaging.

Combining Planar nDEP Focusing and nDEP Trap. Two dimensional traps based on negative dielectrophoresis have been repeatedly reported;[20−22] however, within a microfluidic chip, high reagent consumptions are typically experienced due to particles being repelled out of high electric field gradients. Electrohydrodynamic forces can then be utilized as a tool to increase trapping yields.[23] Planar focusing allows for fast inflow routing of particles toward a given DEP trap. In this article, the focus-and-trap function of a novel electrode geometry is characterized. Simulations are also used to determine the effect of channel height and velocity on the trapping forces.

Theory

The time-averaged DEP force can be written as[13]

$$\vec{F}_{\mathrm{DEP}} = 2\pi\varepsilon_{\mathrm{m}}R^3\mathrm{Re}[\mathrm{CM}(\omega)]\nabla\vec{E}^2(r,\omega) \qquad (1)$$

Here $\vec{F}_{\mathrm{DEP}}$ refers to the dipolar approximation of the DEP force, ε_{m} is the dielectric permittivity of the surrounding medium, R is the radius of the particle, and $\vec{E}(r, \omega)$ is the complex applied electric field, where r is the spatial coordinate of the particle and ω is the angular frequency of the applied field. CM is the Clausius−Mossotti (CM) factor, whose definition depends on the kind of particle considered. A positive CM factor indicates that the DEP force pushes particles toward the electrodes to the electric-field maximum (pDEP) whereas a negative CM factor indicates that the DEP force pushes particles away from the electrodes to the electric field minimum (nDEP).

* To whom correspondence should be addressed. E-mail: joshua.edel@imperial.ac.uk.
[†] Institute of Biomedical Engineering.
[‡] Department of Chemistry.
[§] Chemical Biology Centre.

10.1021/jp808897g CCC: $40.75
Published on Web 01/14/2009

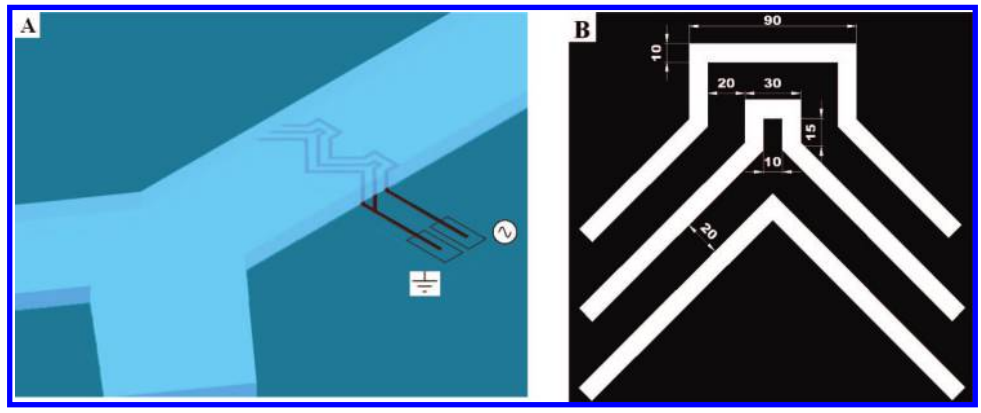

Figure 1. (A) Focused square electrode geometry proposed for cell patterning near a defined surface. (B) Electrode pattern as designed (dimensions are given in microns).

The expression of the time-averaged DEP force (1) is based on the dipolar approximation. Higher order moments may also contribute to the global DEP force. Importantly, in the case of a complex geometry, when nonuniformities in the electrode pattern are commensurate with the size of the particle, higher order moments are likely to be induced.[24] However, in the case of nDEP, particles are pushed out of high gradient regions; the influence of the high order moments is therefore greatly diminished. In addition, high order moments can be neglected in known geometry configurations.[25]

One of the most significant implications of the expression of the DEP force is that it is extremely dependent on geometry through the gradient term$\nabla\vec{E}^2$. Careful design of complex geometries can thus lead to new functions and increased control over particles or cells.[25]

The frequency response of a particle to an externally applied electric field is determined through its CM factor. If we consider a simple dielectric particle with Ohmic conductivity but no dielectric losses immersed in a dielectric medium, the CM factor can be written:

$$\mathrm{CM} = \frac{\varepsilon_p - \varepsilon_m}{\varepsilon_p + 2\varepsilon_m} \tag{2}$$

Here ε_m and ε_p are the complex permittivities of the medium and particle, respectively, and can be each written as

$$\mathrm{Re}(\varepsilon) = \varepsilon + \frac{\sigma}{j\omega} \tag{3}$$

Here Re(ε) is the real part of the complex permittivity, ε is the permittivity of the medium or particle, σ is the conductivity of the medium or particle, and j is $\sqrt{-1}$.

At typical buffer permittivity and conductivity conditions, the medium is more polarizable, which results in the DEP force always being directed toward the electric field minima resulting in negative DEP.

Fabrication and Geometry

Indium Tin Oxide (ITO) Patterning. A microfluidic chip was built using a combination of ITO-coated glass (SPI supplies) and PDMS. The microelectrode design was patterned on an ITO glass substrate using standard photolithography and wet chemical etching. The thickness of the glass substrate was 500 μm and that of the ITO coating was 100 nm. ITO is a metal transparent to visible light and thus optically transparent at the wavelengths of interest.

For ITO etching, AZ 1512HS (MicroChemicals) photoresist was used as a protective layer and exposed to UV light through a lithographic mask (designed by AutoCAD and subsequently printed on a film (JD Phototools)). The exposure dose was adapted to the resist thickness. Nonexposed parts of the resists were then developed with a developer solution AZ 400K (Clariant). An aqueous solution of 4:2:1 $HCl/H_2O/HNO_3$ was prepared for etching ITO. The ITO glass was dipped in the solution for approximately 30 s. After completing the etching process, the substrate was thoroughly rinsed in deionized (DI) water. Finally, the photoresist was removed with acetone. The devices were further cleaned in isopropyl alcohol (IPA) and DI water before being stored in a Petri dish.

PDMS Microchannel. A master mold was fabricated by photolithography on a 4 in. silicon wafer (100) and used as the substrate. The silicon wafer was uniformly coated with SU-8 50 (or SU-8 100) photoresist (coated at 500 rpm for 15 s followed by 3000 rpm for 30 s), soft baked for 15 min at 65 °C and 30 min at 95 °C, exposed with UV light, and developed. The thickness of the microchannel was either 30 or 120 μm. A mixture of PDMS prepolymer (SYLGARD 184 Silicone Elastomer Kit, Dow Corning, Midland, MI) and the curing agent was degassed in a vacuum chamber for 30 min to remove any air bubbles and to ensure complete mixing of the two parts. The mixture was then poured onto the master mold in a Petri dish. It was cured for 12 h at 65 °C on a hotplate. After curing, the PDMS replica was peeled off from the master mold. Fluidic inlets and outlets were punched through the PDMS channel using a syringe needle.

Before PDMS bonding on the ITO patterned glass, the latter was rinsed in 0.5 M KOH solution followed by DI water and nitrogen blowing. The PDMS channel was cleaned using a N_2 gun. Both were plasma oxidized, aligned using a standard microscope and bonded manually. Finally the chips were cured on a hotplate at 95 °C for 5 min.

Packaging. The ITO contact pads were covered with silver glue (RS) and pin connectors (RS) were pressed on it. After curing for a minimum of four hours at room temperature, epoxy (ITW Devcon) was deposited to strengthen the bond between the connectors and microfluidic chip. After curing of the epoxy at 65 °C overnight, electric wires (RS, 0.25 mm^2) were soldered to the pins.

Geometry. A 3D illustration of the design is given in Figure 1A. The geometry itself is inspired by the square electrode design previously reported by Rosenthal et al.[20] The fundamental

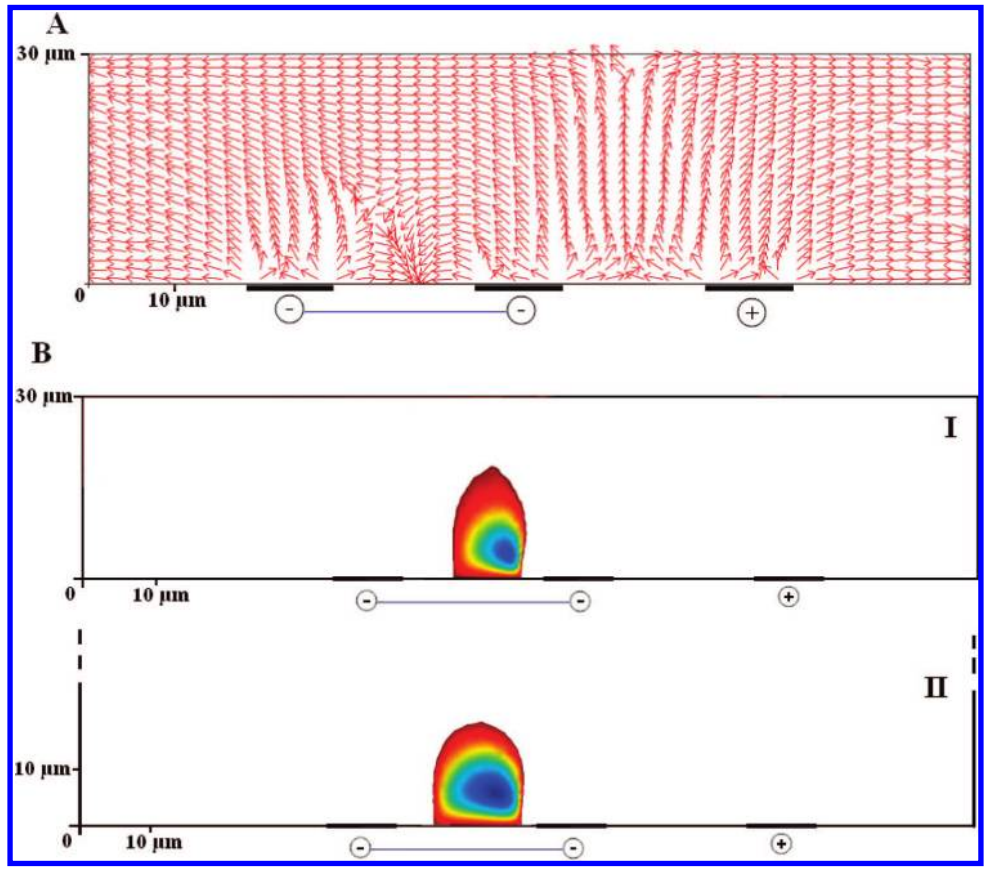

Figure 2. (A) Normalized DEP force direction associated with three line electrodes geometry. (B) Negative component of $|\nabla_z \vec{} E^2|$ in **I**, a shallow channel (30 μm high) geometry, and **II**, a nonshallow (120 μm high) geometry. Blue regions correspond to higher gradients.

difference lies in a focusing element being introduced that is made up of three parallel line electrodes. Importantly, two metal lines are connected to form the cathode. The basic dimensions are given in Figure 1B. Using this geometry, several cages can be aligned or arrayed.

Design Rules. The design rules adopted here are based on the idea that the spacing between cathodes should be at least bigger than the diameter of particles of interest in order to trap them (size selectivity) and to avoid higher-order moments which would make the trapping behavior hard to predict. Nonetheless, a big gap between cathodes translates into decreased electric gradients. For mammalian cell experiments, given the heterogeneities of a cell population, a spacing of 20 μm is a good compromise. The spacing between the anode and inner cathode should be as close as possible to generate high gradients. Here again, 20 μm seems realistic. The width of the electrodes should ensure that fields are not too strongly localized which could lead to cell damage but also not too low to ensure efficient trapping. Ten micrometers is a reasonable value comparable to existing geometries. The angle of the three parallel lines with respect to the flow was chosen as 45°. In real devices, arrays of 5 rows × 4 columns elements were interconnected.

Materials

Flow was initiated via a precision syringe pump (PHD 2000, Harvard Apparatus) using a 1 mL Becton−Dickinson syringe. Bead stock solutions were made with appropriate conductivity by combining appropriate volumes of 18 MΩ cm deionized water containing 0.1% Triton X-100 (to ensure the beads will not stick to the channel surfaces and keep them monodisperse) and phosphate-buffered saline (Sigma Aldrich). Conductivities were measured using a Dist 5 conductivity meter (VWR). Polystyrene (PS) beads (PolySciences) had a density of 1.062 g/cm^3, packaged at 2.5% solids in water. Fluorescent beads (FluoSpheres, Molecular Probe) were 2% solid solutions of polystyrene beads with encapsulated fluorescent dyes (yellow-green fluorescent). Their peak absorption wavelength was 505 nm and their peak emission wavelength was 515 nm.

A function generator (TG2000, Thurlby Thandar Instruments) was connected to the electrodes by BNC cables with adapted wire grip leads gripping the conducting wires of the contact pads to the microelectrodes. A sinusoidal signal with voltage varying between 1 to 20 V_{pp} and a fixed frequency of 10 MHz was applied to the microelectrodes. Imaging and observation was performed using an Olympus IX71 microscope.

Simulations

Principle of the Focusing Element: Leveraging the Downward DEP Force. A DEP cage exists when a particle is forced to go back to its original location (to a potential well) when slightly moved away from its equilibrium. Simulations of such traps require electric field distribution study. They have been performed using the Comsol package based on the finite element method (FEM).

In the 2D model of Figure 2A, the channel height is chosen to be 30 μm. Three line electrodes of width 10 μm have a spacing of 20 μm. The two left electrodes represent the cathode (potential −5 V) while the right electrode is the anode (potential +5 V). The boundary conditions for the fluidics are no-slip on the walls and a null outlet pressure, respectively. The fluid parameters are those of deionized water. The arrows in Figure 2A represent the normalized DEP force direction. Depending

on the location of the particle, the direction of the force varies as follows: (1) Between the anode and cathode, the force is upward toward the center of the electrodes; the particle will be lifted up. This phenomenon is known as DEP levitation. (2) Between the two cathodes the force is downward and pushes particles toward the center of the cathodes; this region defines the DEP trap. If we were to transform the geometry of Figure 2A into a 3D model, we would be in a situation where particles can move between the two cathodes. This forms an open trap which can be used as a focusing element. (3) Outside the outer cathode (the left in Figure 2A), particles are weakly pushed backward (due to the low gradient far from the anode−cathode gap). (4) Outside the anode (the right in Figure 2A), particles are strongly pushed forward.

The device is based on electric field distribution inside a microfluidic channel. It is therefore not surprising that the height of the channel has a tremendous influence on its ability to trap particles. In this section, we analyze the differences between a shallow channel (chosen 30 μm high) in which the electric field is strongly confined and a nonshallow channel (chosen 120 μm high) in which the electric field is weakly confined.

Representation of an nDEP Cage. One representation of a DEP cage in the case of a planar geometry is its downward electric gradient. If z defines the vertical axis of the system, the region for which $|\nabla_z \vec{E}^2|$ is negative will confine particles near a surface. Figures 2B compares qualitatively the surface intensity of this quantity according to the shallowness of the channel. In this figure, particles are coming from the left-hand side. The important parameter is the incoming height of the particle. Indeed, in a device with integrated planar electrodes, the DEP force scales as

$$F_{\mathrm{DEP}} \propto \frac{V^2}{h^3} \tag{4}$$

Here V is the applied potential and h the height of the center of the particle above the substrate. This expression indicates that the strength of the DEP force vanishes quickly with height above the electrodes. In the case where the cage occupies half of the channel height as in the 30 μm high channel (case **I**), there is therefore increased probability of a trapping event with respect to the case of a deep channel.

The distribution of the downward force also varies. While it is strongly located on the edge of the inner cathode (the blue region corresponds to higher gradients) for a shallow channel (case **I**), it is more evenly distributed for a deeper channel (case **II**).

Influence of the Height of the Channel. As predicted in Figure 2A, the outer electrode will lift particles up, creating a DEP barrier. If a particle is uplifted too much, it will not enter the focusing region and will be able to escape. Simulations show the relative magnitude of this barrier $\nabla_z \vec{E}^2$ at 5 μm above the substrate as a function of channel height (Figure 3). For a shallow 30 μm high channel, the barrier is about 2.5 times weaker than for a 120 μm high channel.

This can be explained by the restriction of the field due to the small vertical extension. In other words, there is confinement of the electric field nonuniformities near the adjacent anode and cathode.[25] This difference in barrier height is sufficient to change trapping methodologies according to channel height as detailed in the results section. Figure 4 shows the maximum barrier height as a function of channel height. The potential was kept constant at 10 $V_{pp.}$ The figure reflects the degree of confinement of the electric field: the shallower the channel, the lower the DEP barrier. For channel heights of 200 μm and above, there is no more confinement and the barrier height is maximum.

Results and Discussion

In shallow channels, the methodology for trapping particles is to sequentially activate the flow of beads (at a desired concentration) with the syringe pump at a flow rate suitable for trapping (in μL/min) and turn on the electric field. Beads flowing close enough to the electrodes will be automatically trapped. The trapped beads can accumulate in the DEP cage until the focusing region is completely filled (beads accumulate and form lines). After turning off the field, beads are carried away by the flow.

In nonshallow channels, particles cannot enter the trap due to the aforementioned "barrier". The field has to be switched on manually when beads are located in-between the two cathode line electrodes. Importantly, in this case trapped beads cannot interact with untrapped ones while the electric field is present. The manual trapping requires a feedback that can be simply visual using a microscope eyepiece or a camera. Figure 5 displays a series of pictures showing a focus-and-trap event of a single polystyrene bead in a nonshallow channel.

Velocity Analysis. Whether particles actually contact the surface in the presented focusing element can be studied via velocity analyses of single particle. This also gives more insight into the principle of operation. A Cascade II camera (Photometrics, Roper Scientific, Inc.) was used to record fluorescence movies of flowing fluorescent beads. A maximum of 29 frames per second was used to record 512 × 512 pixel movies. The image postprocessing of the individual frames of the recorded movies was performed using Matlab.

Figure 6 represents a typical velocity curve for a fluorescent bead flowing sufficiently close to the patterned surface to get focused and subsequently trapped.

Four regions can be highlighted on this graph:

1. When the particle is incoming, its velocity is constant and there is no polarization effect from the electric field.

2. The particle reaches the edge of the outer ITO line, its velocity increases quickly to nearly twice its previous speed.

3. Approaching the inner ITO cathode, the particle is quickly slowed down and gets focused.

4. The particle is finally trapped and stops.

Interestingly, the velocity profile is rather flat in the focusing region and amounts to around 60% of the incoming speed. This decrease in speed before the trapping region increases the probability of a trapping event and hence trapping efficiency. The velocity profile also clearly rules out contact with a surface in which case the speed would be either very low (permanent contact) or fluctuating (particles bouncing). In fact, contact is prevented by the hydrodynamic uplift and the focusing speed mainly depends on the angle of the focusing line electrodes as well as the radius of the particles (although no experiments have been performed to prove this point). This focusing velocity could thus be used for size determination of a population of cells/particles.

Trapping and Holding Force. Trapping and holding force of an nDEP trap represent a figure of merit. For the shallow devices, the trapping force is the threshold voltage at a given flow rate under which flowing spheres cannot be focused and trapped anymore. For the nonshallow devices, the electric field is turned on manually when spheres are passing within the two cathodes and the same definition applies.

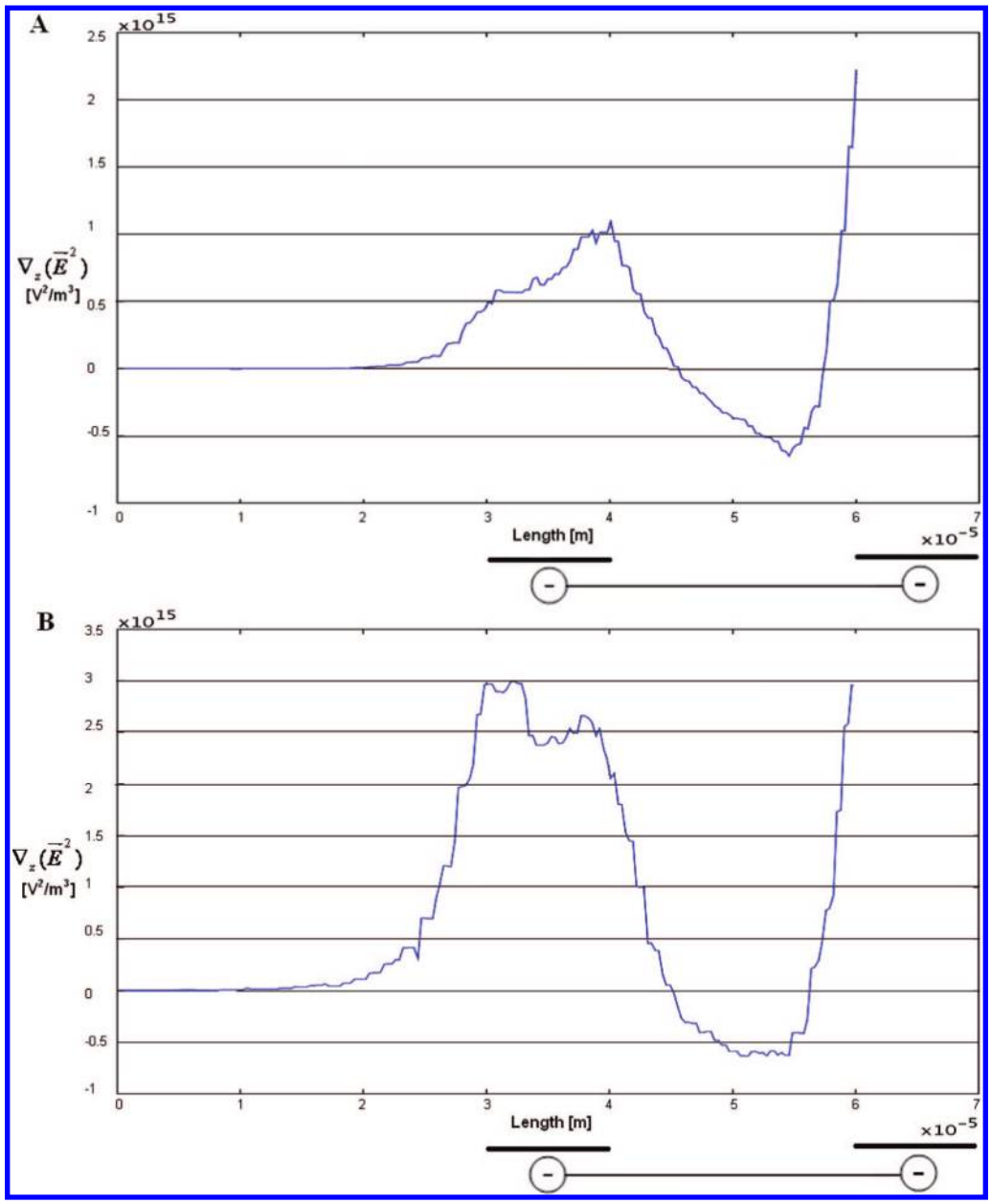

Figure 3. Cross-section of $\nabla_z(\vec{E}^2)$ 5 μm over the cathode line electrodes in (A) a shallow 30 μm high channel and (B) a 120 μm high channel.

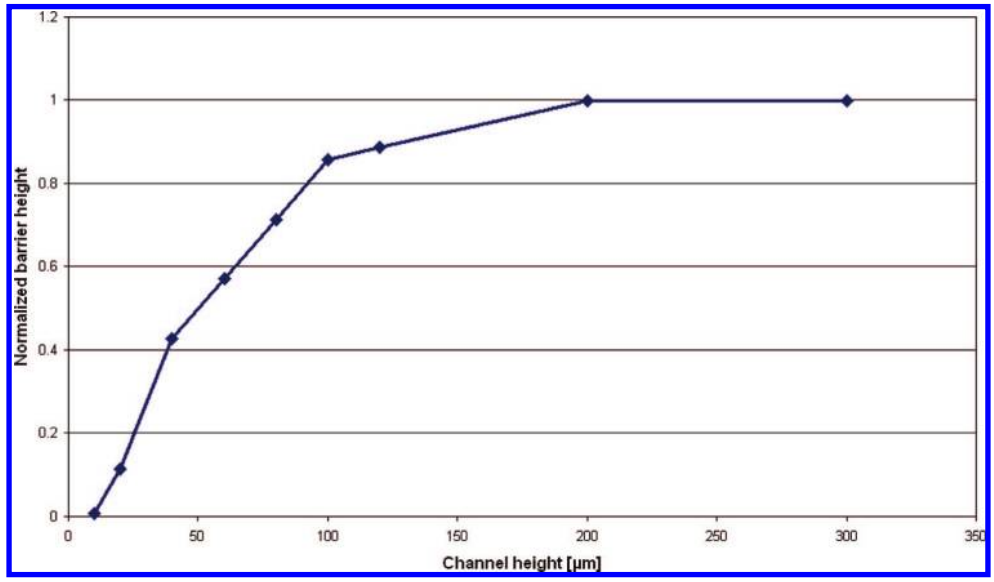

Figure 4. Normalized DEP barrier height (upward DEP force) over the first line electrode as a function of channel height at constant voltage.

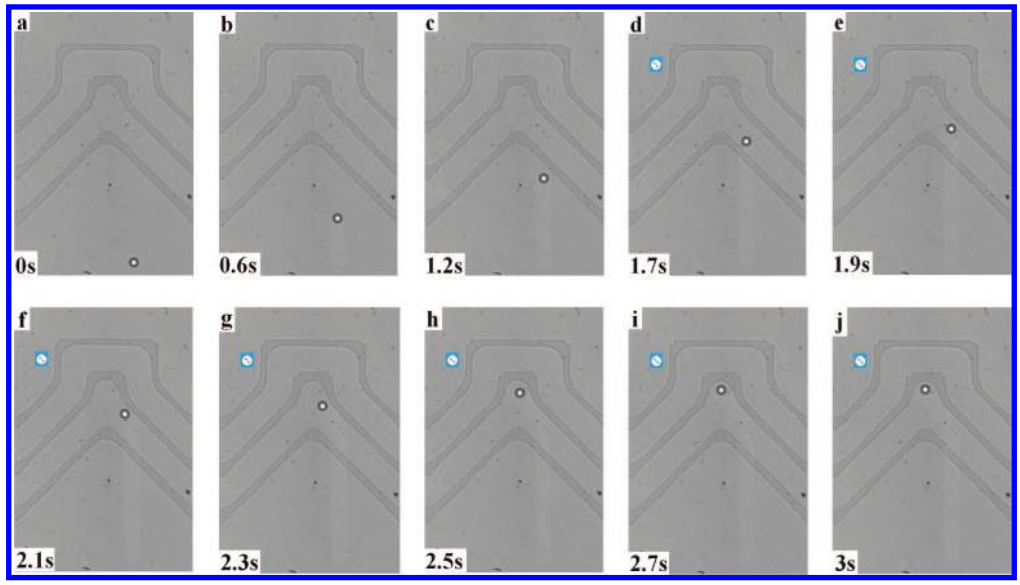

Figure 5. Planar focusing and trapping in a nonshallow channel. (a−c) Incoming PS bead of 10 μm in diameter. (d) The electric field is manually turned on when the bead enters the gap between the two cathodes. (e−h) The bead is focused. (i,j) The bead finally becomes trapped.

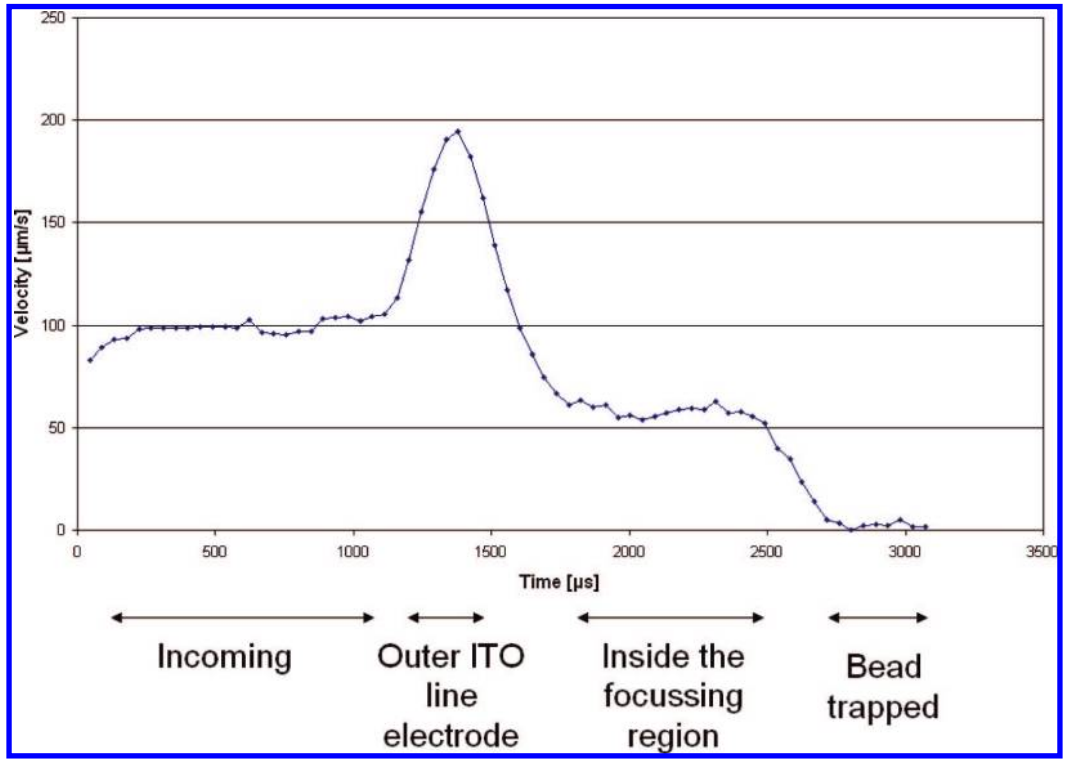

Figure 6. Velocity of a single particle being focused and subsequently trapped in the DEP cage.

The holding force is the threshold voltage at a given flow rate under which trapped spheres get carried away by the flow.

Quantifying the Trapping Force. Chips were cleaned by injecting ethanol for roughly 5 min. After this step, a high density of beads (around 100 beads/μL) was injected inside the microchannel and the flow rate was set at a constant value. The electric field was a sinusoidal wave of frequency 10 MHz and low amplitude. After waiting for the flow to be steady, the voltage was increased by steps of 1 V_{pp}. The threshold voltage for which particles get focused and trapped corresponds to the trapping force. This was visualized using a high speed camera (Phantom v5.1, Vision Research).

Quantifying the Holding Force. Particles are now assumed to be already trapped. The electric field was a sine wave of frequency 10 MHz and the amplitude was set much higher than the trapping threshold. The flow rate was set at a constant value. After waiting for the flow to be steady, the voltage was decreased by steps of 1 V_{pp}. The threshold voltage for which particles escape corresponds to the holding force. The 1 V_{pp} step is sufficiently big that most beads trapped in different cages (in the case of a trap array) would escape at that same threshold.

The curves in Figure 7 showing the trapping and holding force were obtained with 30 μm spacing between electrodes in a 120 μm high channel geometry. The conductivity of the nonfluorescent bead buffer was adjusted to 0.18 S/m. The curves show a quadratic trend as expected from eq 1: while the drag force increases linearly with the flow velocity, the DEP force increases in a quadratic manner with the applied voltage. The functional

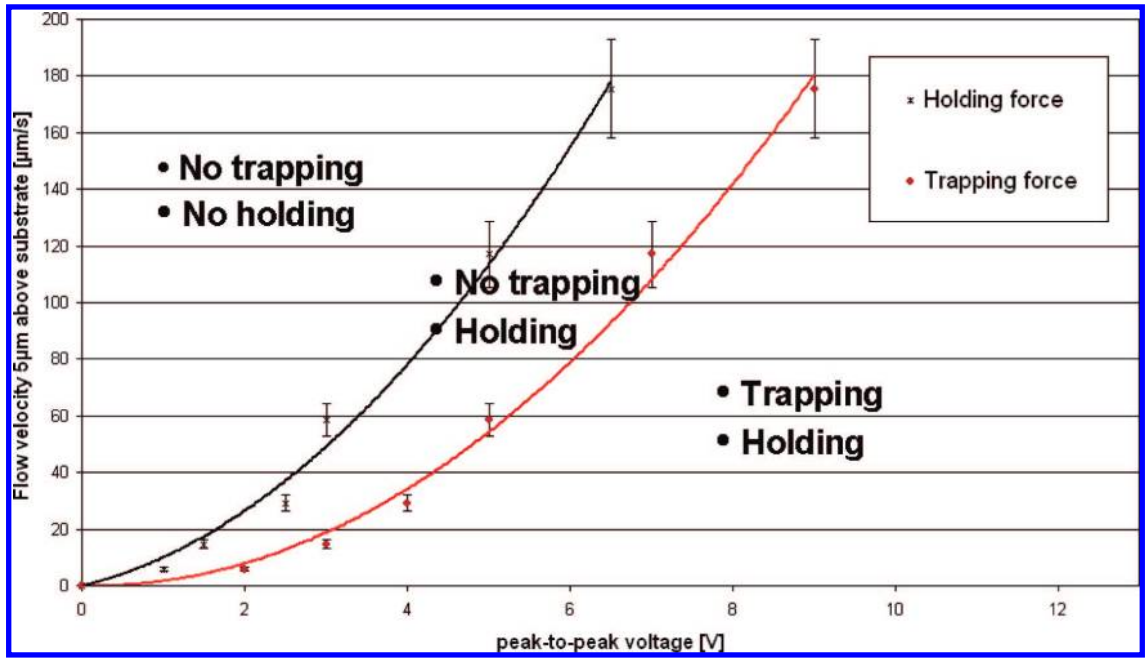

Figure 7. Trapping and holding regions according to flow velocity 5 μm above the substrate and peak-to-peak voltage.

form of the fit in Figure 7 is $y = Ax^2 + Bx$. The three regions it delimitates are as follows. For low flow velocities and high voltage, beads can be trapped and held. At a certain velocity threshold, spheres can be held but not trapped. For high flow velocities and low voltage, spheres can neither be trapped nor held.

The direct observation made in Figure 7 is that the trapping force is weaker than the holding force. These two distinct curves can be accounted for by the balance between drag flow and the counteracting DEP force. For the trapping force, a bead is in motion and has to be deviated until it reaches a potential well. After reaching its stable position in a trap, the bead experiences a stronger DEP force and can therefore withstand stronger flow rates (i.e., the holding force is higher). In order to compare the holding force with the square electrode design, extrapolations from the data provided in (20) are performed. At a peak voltage of 5 V and for corrected electrode spacing and channel geometry, the presented design is found only 20% weaker.

Single-particle trapping can be achieved using this design by working near the holding force threshold. The device can also be used in high-throughput format by increasing the flow rate and adjusting the field to just above the trapping threshold voltage. For cellular work, the use of a low electric field strength is a requirement. Many studies suggest the maximum field strength leading to acceptable transmembrane loading is in the order of 10^6 V/m.[16,25,26] Other interesting applications of the developed system include line patterning of particles, focusing particles in stream lines or creating arrays.

The trapping yield for previously reported devices is typically very low (<1%) because the surface has to be initially fully covered by particles. While this is a rather quick step, the untrapped particles will for the most part not be used and therefore constitute waste. Using the focusing element would allow to dramatically improve the trapping yield which was found as high as 50% in favorable conditions (shallow channel, low flow rate and high voltage).

Conclusions

A novel geometry for focusing particles or cells in-flow near a defined surface has been presented. The speed of operation is substantially higher than previously reported designs for trapping as practical flow velocities are high (up to hundreds of micrometers per second). Simulations have shown the principle of a semiopen trap and highlighted the influence of channel height over the trap strength and operation. The trapping and holding force of polystyrene microbeads have been quantified in terms of balance between field strength and flow velocity. The holding force was found only slightly weaker than previously reported planar geometries. Using this novel focus-and-trap element for cell experiments would ensure cells do not get into direct contact with metal electrodes which avoids charging and improves cell viability.

References and Notes

(1) Cheng, I. F.; Chang, H. C.; Hou, D.; Chang, H. C. *Biomicrofluidics* **2007**, *1*, 15.
(2) Choi, S.; Park, J. K. *Lab Chip* **2005**, *5*, 1161.
(3) Holmes, D.; Morgan, H.; Green, N. G. *Biosens. Bioelectron.* **2006**, *21*, 1621.
(4) Wild, D. *The immunoassay handbook*, 3rd ed.; Elsevier: New York, 2005
(5) Wiklund, M.; Toivonen, J.; Tirri, M.; Hänninen, P.; Hertz, H. M. *J. Appl. Phys.* **2004**, *96*, 1242.
(6) Gordon, E. M.; Barrett, R. W.; Dower, W. J.; Fodor, S. P.; Gallop, M. A. *J. Med. Chem.* **1994**, *37*, 1385.
(7) Pregibon, D. C.; Toner, M.; Doyle, P. S. *Science.* **2007**, *315*, 1393.
(8) Tourovskaia, A.; Figueroa-Masot, X.; Folch, A. *Lab Chip* **2005**, *5*, 14.
(9) Khine, M.; Lau, A.; Ionescu-Zanetti, C.; Seo, J.; Lee, L. P. *Lab Chip* **2005**, *5*, 38.
(10) Holmes, D.; Sandison, M. E.; Green, N. G.; Morgan, H. *IEE Proc.: Nanobiotechnol.* **2005**, *152*, 129.
(11) Muller, T.; Gradl, G.; Howitz, S.; Shirley, S.; Schnelle, T.; Fuhr, G. *Biosens. Bioelectron.* **1999**, *14*, 247.
(12) Wang, L. S.; Flanagan, L.; Lee, A. P. *J. Microelectromech. Syst.* **2007**, *16*, 454.
(13) Pohl, H. A. *Dielectrophoresis*; Cambridge University Press: New York, 1978
(14) Fuchs, A. B.; Romani, A.; Freida, D.; Medoro, G.; Abonnenc, M.; Altomare, L.; Chartier, I.; Guergour, D.; Villiers, C.; Marche, P. N.; Tartagni, M.; Guerrieri, R.; Chatelain, F.; Manaresi, N. *Lab Chip* **2006**, *6*, 121.
(15) Docoslis, A.; Kalogerakis, N.; Behie, L. A. *Cytotechnology.* **1999**, *30*, 133.
(16) Fuhr, G.; Glasser, H.; Muller, T.; Schnelle, T. *Biochim. Biophys. Acta* **1994**, *1201*, 353.
(17) Archer, S.; Li, T. T.; Evans, A. T.; Britland, S. T.; Morgan, H. *Biochem. Biophys.* **1999**, *257*, 687.

(18) Chu, H.; Doh, I.; Cho, Y. H. *21st IEEE International Conference on Micro Electro Mechanical Systems, Technical Digest*; IEEE: New York, 2008; p 622.
(19) Yu, C. H.; Vykoukal, J.; Vykoukal, D. M.; Schwartz, J. A.; Shi, L.; Gascoyne, P. R. C. *J. Microelectromech. Syst.* **2005**, *14*, 480.
(20) Rosenthal, A.; Voldman, J. *Biophys. J.* **2005**, *88*, 2193.
(21) Ozkan, M.; Pisanic, T.; Scheel, J.; Barlow, C.; Esener, S.; Bhatia, S. N. *Langmuir.* **2003**, *19*, 1532.
(22) Hughes, M. P. *Biophys. J.* **1999**, *77*, 516.
(23) Heida, T.; Rutten, W. L. C.; Marani, E. *J. Phys. D: Appl. Phys.* **2002**, *35*, 1592.
(24) Voldman, J.; Braff, R. A.; Toner, M.; Gray, M. L.; Schmidt, M. A. *Biophys. J.* **2001**, *80*, 531.
(25) Albrecht, D. R.; Sah, R. L.; Bhatia, S. N. *Biophys. J.* **2004**, *87*, 2131.
(26) Arnold, W. M.; Franich, N. R. *Curr. Appl. Phys.* **2006**, *6*, 371.

JP808897G